JACS
JOURNAL OF THE AMERICAN CHEMICAL SOCIETY
Article
pubs.acs.org/JACS

A Generalizable Platform for Interrogating Target- and Signal-Specific Consequences of Electrophilic Modifications in Redox-Dependent Cell Signaling

Hong-Yu Lin,[†] Joseph A. Haegele,[†] Michael T. Disare,[†] Qishan Lin,[§] and Yimon Aye*[,†,‡]

[†]Department of Chemistry and Chemical Biology, Cornell University, Ithaca, New York 14853, United States
[‡]Department of Biochemistry, Weill Cornell Medical College, New York, New York 10065, United States
[§]Proteomics/Mass Spectrometry Facility, Center for Functional Genomics, University of Albany, Rensselaer, New York 12144, United States

Supporting Information

ABSTRACT: Despite the known propensity of small-molecule electrophiles to react with numerous cysteine-active proteins, biological actions of individual signal inducers have emerged to be chemotype-specific. To pinpoint and quantify the impacts of modifying one target out of the whole proteome, we develop a target-protein-personalized "electrophile toolbox" with which specific intracellular targets can be selectively modified at a precise time by specific reactive signals. This general methodology, T-REX (targetable reactive electrophiles and oxidants), is established by (1) constructing a platform that can deliver a range of electronic and sterically different bioactive lipid-derived signaling electrophiles to specific proteins in cells; (2) probing the kinetics of targeted delivery concept, which revealed that targeting efficiency in cells is largely driven by initial on-rate of alkylation; and (3) evaluating the consequences of protein-target- and small-molecule-signal-specific modifications on the strength of downstream signaling. These data show that T-REX allows quantitative interrogations into the extent to which the Nrf2 transcription factor-dependent antioxidant response element (ARE) signaling is activated by selective electrophilic modifications on Keap1 protein, one of several redox-sensitive regulators of the Nrf2−ARE axis. The results document Keap1 as a promiscuous electrophile-responsive sensor able to respond with similar efficiencies to discrete electrophilic signals, promoting comparable strength of Nrf2−ARE induction. T-REX is also able to elicit cell activation in cases in which whole-cell electrophile flooding fails to stimulate ARE induction prior to causing cytotoxicity. The platform presents a previously unavailable opportunity to elucidate the functional consequences of small-molecule-signal- and protein-target-specific electrophilic modifications in an otherwise unaffected cellular background.

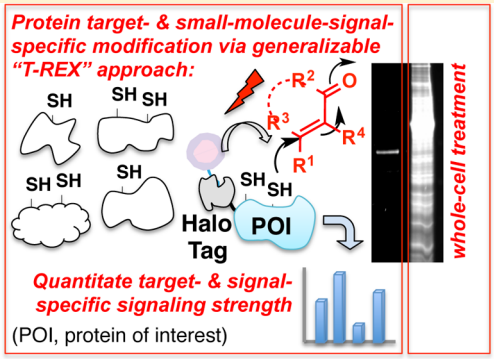

INTRODUCTION

Lipid-derived electrophiles (LDEs) are a diverse class of endogenous small molecules capable of covalently modifying proteins.[1] The LDE-derived post-translational modifications have shown growing importance in regulating redox-dependent intracellular communications.[1,2] The biological consequences of LDE-derived protein modifications are most associated with a wide range of cytoprotective signaling responses.[1−3] However, unlike conventional enzyme-assisted modifications such as phosphosignaling,[2] much less is known about the mechanisms by which diffusible small-molecule chemical messengers nonenzymatically orchestrate signal susceptibility of specific proteins in a cell or modulate the strength of signal propagation downstream.[1,3] Essentially an innumerable array of chemically diverse LDEs is available. However, how a specific protein target/pathway deals with reactive LDEs, and whether timing and specificity differ across various LDE classes remain unclear.[3]

Individual LDE signaling events have traditionally been studied by "overload" methodologies in which cells are swamped with reactive signal-inducers and a particular response is read out. However, when the entire cell is exposed to a reactive signal, numerous proteins [>700 in the case of a well-known signaling electrophile 4-hydroxynonenal (HNE)][4a] are modified simultaneously. Thus, precise information linking varied chemical architectures of LDE signals and/or timing of modifications to phenotypic responses triggered by modifying specific protein targets in a cell is not easily attainable.[1,3,4] Recent innovations in quantitative proteomics involving global treatment with signaling electrophiles have provided powerful insights into relative cysteine (Cys) reactivity within the human proteome.[4] However, even these innovative approaches can only rank reactivities, and lack the ability to perturb specific

Received: December 30, 2014
Published: April 24, 2015

DOI: 10.1021/ja5132648
J. Am. Chem. Soc. 2015, 137, 6232−6244

proteins or forge a link between specific target modification by individual LDEs and specific response downstream.

In addition to the physiologic relevance of endogenous LDE modifications in redox-linked cell signaling,[1,3,4] small-molecule drugs with electrophilic motifs analogous to those manifested in LDEs are also increasingly recognized for pharmacologic benefits.[5] Importantly, existing data in the field of LDE signaling show evidence of distinct biological specificity and responses elicited by myriad LDEs featuring chemical structural resemblance of varying degrees.[6] To date, however, the mechanisms by which chemically discrete small-molecule redox-mediators establish their phenotypic bioreactivity on a single protein target at a given instant in cells, and how these modest modifications on specific targets in turn influence the magnitude of downstream signaling, remains shrouded in mystery[1,3−7](Figure 1a).

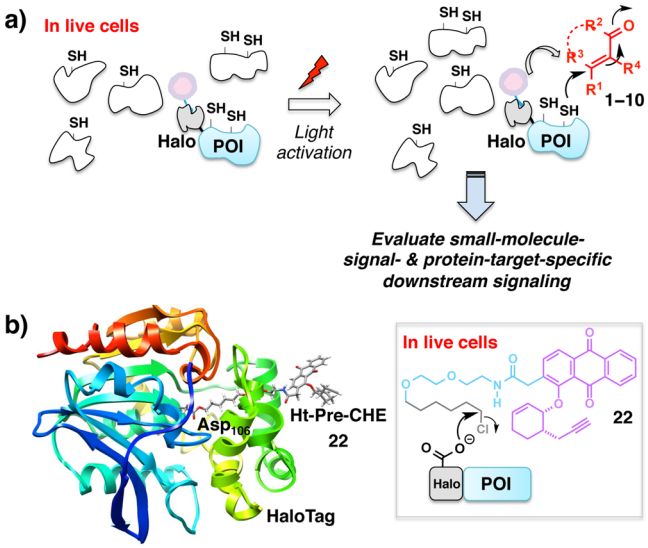

Figure 1. (a) The generalizable T-REX (targetable reactive electrophiles and oxidants) approach selectively delivers a reactive signaling electrophile of choice to specific redox-sensor protein of interest (POI) at a precise time in live cells. Photocaged precursor (pink sphere) is covalently linked to HaloTag fused to POI. Low-energy light activation (365 nm, 0.6 mW/cm^2) liberates the desired reactive signal in stoichiometric amount to the microenvironment of the POI enabling targeted modification. The spatiotemporally precise modification upstream in turn enables quantitative evaluation of single- and target-specific response downstream. (b) Energy minimized model of Halo (PDB: 1BN6) with covalently bound caged precursor Ht-Pre-CHE **22** showed the caged motif is solvent exposed. Inset exemplifies covalent conjugation of **22** to the active site Asp residue on Halo.

Michael acceptors, such as endogenous LDEs[1b,3,4,6] and cyclopentenone prostaglandin metabolites,[1a,3a,8] constitute an important class of small-molecule electrophilic inducers for the transcription factor "nuclear factor-erythroid 2 p45-related factor 2" (Nrf2)-regulated "antioxidant response element" (ARE)-driven genes.[3a,9] However, the regulatory mechanisms of Nrf2−ARE signaling axis are multimodal,[9a] many of the upstream pathways are mediated by proteins that are reportedly redox-sensitive (Figure 2, inset).[10] As a cytosolic anchor of Nrf2 and an adaptor protein for Cul3-based ubiquitin E3 ligase complex for Nrf2, the "Kelch-like ECH-associating protein 1" (Keap1)[11] helps to maintain a low steady-state level of Nrf2 by constitutively ushering Nrf2 to be degraded by the

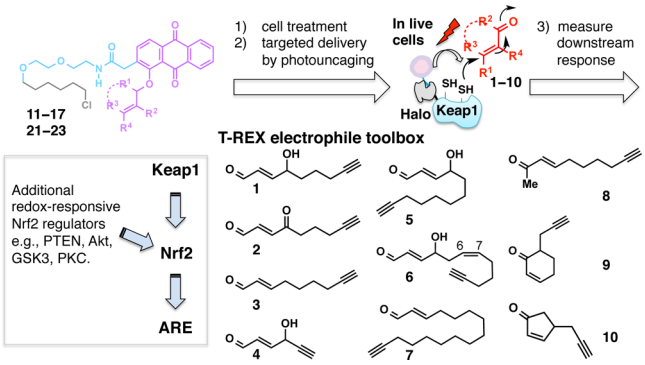

Figure 2. T-REX electrophile toolbox enables assessment of downstream signaling strength triggered by target-specific delivery of specific bioactive LDEs (**1**−**10**) to specific proteins in cells (e.g., Keap1) at a precise time. Inset: The simplified model for Nrf2−ARE pathway. The downstream phenotypic responses, Nrf2 stabilization and ARE upregulation, are observed from whole-cell LDE flooding. Electrophilic modifications of various upstream redox-sensitive targets, including Keap1, PTEN, Akt, GSK3, PKC, etc., have been implicated to play roles in modulating Nrf2−ARE signaling. Using T-REX, this study directly probes the Nrf2−ARE signaling strength selectively elicited by LDE-signal-specific and Keap1-protein-specific electrophilic modifications in an otherwise unmodified proteome.

proteasome.[10,11] Whole-cell electrophile flooding results in blockage of Nrf2 degradation and consequent ARE upregulation.[9−11] Since Keap1 is a highly cysteine rich protein, well-known in vitro to form covalent adducts with myriad electrophiles including LDEs, the Nrf2−ARE activation observed subsequent to whole-cell electrophile treatment is in part attributed to Keap1 operating as a redox-dependent ARE-regulator through direct interaction with small-molecule electrophiles.[11] However, multiple Keap1-independent electrophile-responsive mechanisms of Nrf2−ARE regulation are known.[9−11] Many upstream regulators of Nrf2−ARE axis (Figure 2, inset) are also shown to covalently bind LDEs such as 4-hydroxynonenal (HNE).[10,11e] Developing a quantitative understanding of the Nrf2−ARE pathway has recently proven attractive with the emergence of electrophilic drugs such as BG-12 (Tecfidera) that are thought to function in part through activation of ARE response by Keap1 alkylation.[5a,b]

We recently communicated a proof of concept demonstrating selective delivery of the most well-studied LDE, HNE-(alkyne) **1** (Scheme S1, Supporting Information), to redox-active proteins in live mammalian cells at a precise time.[12] We subsequently extended this method to interrogate whether specific HNEylation of Keap1 in low stoichiometry could elicit an ARE response, or whether subsidiary factors were required.[13] These pilot studies unambiguously demonstrated that Keap1 is a key redox sensor along the Nrf2−ARE cascade, specifically, HNEylation of Keap1 is alone biologically sufficient to elicit an ARE response of magnitude similar to that observed under whole-cell HNE flooding.[13] Thus, T-REX allows quantitation of the relative strength of downstream signaling selectively induced by Keap1-alone HNEylation, information not easily obtainable by whole-cell LDE treatment approaches.[1,3−7] Notably, however, widely different biologic responses are reportedly elicited by whole-cell stimulation with structurally different LDEs.[6] Unfortunately, diffferent chemical properties of each individual LDE also result in hitting different sets of targets beyond Keap1, thereby giving rise to different off-target responses. Thus, achieving a new

DOI: 10.1021/ja5132648
J. Am. Chem. Soc. 2015, 137, 6232−6244

ability to precisely correlate single-LDE-signal-specific targeted perturbations to specific biological responses of interest is important. Our attention thus turned to generalization of the T-REX strategy to a broad array of lipid-derived signaling electrophiles. We thus not only set out to quantitatively understand the tolerance, scope, and mechanistic basis of the unique T-REX tool, but also sought to transform this newly developed concept into a generalizable platform with which we can quantitate the magnitude of signaling response that can be activated by specific chemical signals selectively delivered to specific proteins in living cells (Figure 1a).

Despite the apparently privileged role of Keap1 in reactive small-molecule sensing,[11] the functional relationship between electrophilicity/structural variations within small-molecule Michael acceptors and potency of ARE induction downstream remains largely unclear. There is currently no coherent view of the structure−activity relationship of reactive electrophiles and specific biological responses, such as ARE regulation, through precise target modifications in the literature. Indeed it has been challenging to precisely address this issue because ARE induction depends on a number of variables, including cell permeability, protein target promiscuity, stability, and toxicity of discrete small-molecule signals, beyond their ability to modify Keap1 (and other known redox-sensitive regulators of the Nrf2−ARE axis[10,11e]). Some reports implicate that a range of structurally similar small-molecule electrophilic entities all elicit similar levels of ARE induction, and hence Keap1 has evolved to be a promiscuous sensor in responding to myriad structurally discrete inducers.[14] On the other hand, ranges as large as ∼50−1000-fold differences in the downstream gene activation potencies have been implicated across structurally similar enal- and enone-based inducers,[5e,15] possibly suggesting that Keap1 is a more discerning sensor of electrophiles. However, since all these data were collected using global electrophile stimulation, a condition in which multiple redox-sensitive ARE-regulators are modified by the reactive signals,[4,10] the ultimate phenotypic ARE response is less likely to be a true representative of signal- and target-specific ARE induction strength. T-REX is thus suited to parse out these outstanding complexities in the field. Herein we disclose the results of our interrogations into T-REX-assisted targeted delivery of reactive LDEs **1**−**10** (Figure 2) selectively to Keap1 with spatiotemporal regulation, and quantitative evaluations of how these signal- and target-specific modest modifications specifically translate to modulate the strength of Nrf2−ARE signal propagation.

RESULTS

Construction of T-REX Electrophile Toolbox. We first focused on alkenal-based linear Michael acceptors **2**−**7** (Figure 2) that have been implicated to regulate various cellular functions and cytoprotective responses.[3a,6] The alkyne functionalization at the chain terminus enables tracking of proteins covalently bound (via HaloTag,[16] Figure 1b) to the caged precursors, or quantitative assessment of the extent to which specific proteins are modified by the liberated electrophile (by using Click coupling[17] with Cy5-azide).[12] Photocaged precursors to alkyne-functionalized alkenals, ONE **2**, dHNE **3**, HHE **4**, HDE **5**, HDDE **6**, and 2-HD **7** (**11**−**16**, Figure 2) (Scheme S2−S7), were selected. These alkenals not only regulate various physiologic responses,[3a,6] but also cover a range of chain lengths and electronically diverse Michael acceptors, allowing us to investigate the tolerance of T-REX.

Our initial synthetic strategy was centered upon extending the previously reported synthesis of Ht-Pre-HNE **17**[12] (Figure 3a). In this approach, Williamson ether synthesis[18] furnishes

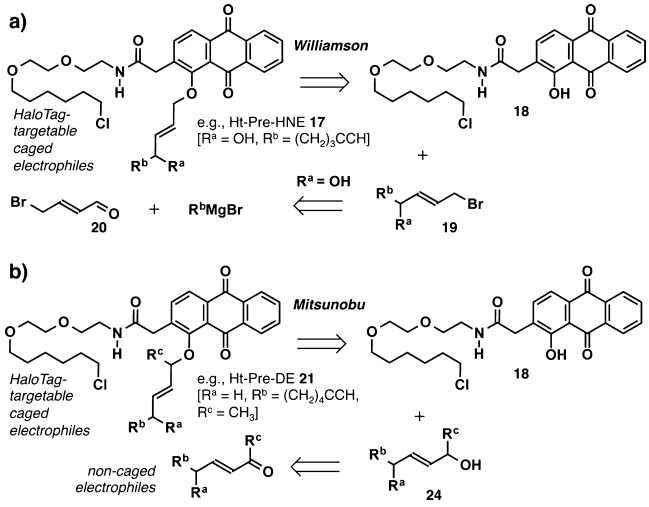

Figure 3. Synthetic strategies for the construction of T-REX electrophile toolbox. (a) The Williamson ether synthesis approach. (b) The Mitsunobu approach. See also Scheme S2−S10. All compounds are racemic where applicable.

the caged electrophile from anthraquinone **18** and allylic bromide **19**, accessed from known aldehyde **20** and the corresponding Grignard reagent, or other simple precursors. Syntheses of HaloTag-targetable caged precursors: Ht-Pre-HNE **17**, Ht-Pre-dHNE **12**, Ht-Pre-HHE **13**, Ht-Pre-HDE **14**, Ht-Pre-HDDE **15**, and Ht-Pre-2-HD **16** were successfully accomplished using this approach (Scheme S3−S7). Ht-Pre-ONE **11** was synthesized via allylic oxidation of **17** (Scheme S2).

We were also motivated to ultimately expand T-REX approach to delivering enones, both linear and cyclic (**8**−**10**, Figure 2). However, enones potentially represent a challenge because (1) they are less reactive than enals, and (2) the photouncaging method used in T-REX has not been well established for liberating enones in aqueous media.[12,19] Cyclohexenone-derived systems serve as simplified representatives of electrophilic pharmacophores such as oleanane-derived synthetic triterpenoids CDDOs,[5c,d,20] whereas cyclopentenone-based delivery platforms can serve as simple models of isoprostanes and prostaglandins, an important class of endogenous signaling molecules.[8,21] Keap1 is indeed a postulated cellular target of these enone-based Michael acceptors.[20,21] Ht-Pre-DE **21**, Ht-Pre-CHE **22**, and Ht-Pre-CPE **23** were thus constructed.

The synthesis of caged enones necessitated a new synthetic strategy because Williamson ether synthesis was found to be not efficient with secondary allyl bromides. Williamson coupling is also not amenable to the synthesis of corresponding noncaged alkyne-functionalized enones **8**−**10**, analysis of which should prove useful for comparing the signaling impact of T-REX approach to that achieved from whole-cell electrophile soaking. We thus developed a more general method (Figure 3b) in which the caged electrophile was derived from anthraquione **18** and alcohol **24** via Mitsunobu reaction.[22] Using this strategy, Ht-Pre-DE **21**, Ht-Pre-CHE **22**, and Ht-Pre-CPE **23** were prepared efficiently (Scheme S8−S10).

DOI: 10.1021/ja5132648
J. Am. Chem. Soc. 2015, 137, 6232−6244

Compared to the previously reported Williamson coupling-based strategy,[12] the new Mitsunobu-based approach provided simultaneous access to both caged and noncaged electrophiles. For instance, Ht-Pre-CHE **22** was constructed directly from silylated CHE **9** (Scheme S9). On the other hand, Ht-Pre-CPE **23** was synthesized from the alcohol-derivative of enone CPE **10**, which was simpler to prepare than the enone itself (Scheme S10).

Assessment of Biocompatible Photouncaging Efficiency. We found that photouncaging caged precursors, **11**–**17** and **21**–**23**, covalently bound in 1:1 stoichiometry to HaloTag in solution was an efficacious way to evaluate the kinetics of photoinduced LDE liberation. By using in-gel fluorescence analysis, the time-dependent Cy5 signal depletion was measured subsequent to photouncaging and Click coupling (Figure 4 and S1). The release kinetics showed controlled rapid

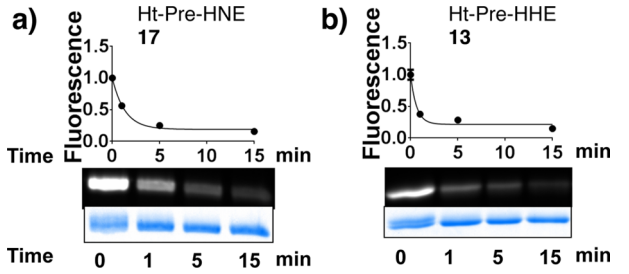

Figure 4. Light-activatable release efficiencies of HNE **1** and HHE **4** from (a) **17** and (b) **13** covalently bound to HaloTag in solution, respectively. See also Figure S1 and Table S1.

electrophile liberation of all enals **1**–**6** at 37 °C (pH 7.6) ($t_{1/2}$ < 1 min for most cases) (Table S1, Figure 4 and S1). The release of 2-HD **7** under standard conditions was however inefficient (Figure S1e). But when the experiment was replicated under denaturing conditions in which HaloTag prebound with Ht-Pre-2-HD **16** was treated with 1% SDS before photouncaging, a release rate ($t_{1/2}$) of ∼0.6 min was measured for 2-HD **7** (Figure S1f), a value similar to that of other enals **1**–**6** (Table S1). This observation suggested that the long aliphatic chain within the liberated 2-HD **7** (and/or within the "precursor **16**–HaloTag" complex) nonspecifically binds to HaloTag presumably through hydrophobic interactions,[16] allowing covalent bond formation between HaloTag and 2-HD **7** to occur subsequent to photolibeartion of **7** from the caged precursor **16**. Based off these findings, Ht-Pre-2-HD **16** was omitted from subsequent studies. On the other hand, all three enones studied **8**–**10** were liberated efficiently. The release of enone DE **8** from Ht-Pre-DE **21** was ∼twice as fast ($t_{1/2}$ ∼ 0.3 min) as enals **1**, **3**–**6** from their corresponding precursors (**17**, **12**–**15**), respectively (Table S1, Figure S1). The cyclic enones CHE **9** and CPE **10** were also liberated successfully (Table S1, Figure S1). These data collectively documented that HaloTag is largely unreactive to enals and enones, and thus serves as a good point source of electrophilic signals. Energy minimization analysis (Macromodel, Schrödinger Inc.) (Figure 1b) further showed that the 15-atom linker renders the inert caged motif solvent-exposed, enabling release of the reactive signals to the surrounding microenvironment of the target protein fused to HaloTag.

Alkylation Rate Profiles. We developed T-REX on the premise that targeted delivery in cells enables rapid accumulation of liberated electrophile within the coordination sphere of the target protein. The redox-sensitive target and the reactive chemical entity thus constitute a solvent-caged "target–signal encounter complex"[23]. The liberated reactive particle was expected to partition between quasi-intramolecular interaction with the target, and diffusion away from the target protein to the bulk medium where it was expected to by scavenged by cellular thiols such as glutathione (GSH) present in mM quantities.[24a] Since the reactive small molecule can only be generated maximally in stoichiometry with respect to the target protein (Figure 1b), side reaction with proteins other than the target was expected to be low.[24]

We initially examined the alkylation rate profiles of purified recombinant human His_6-Keap1 (Table S2) protein with various LDEs of differing electrophilicity. The relative alkylation rates of Michael acceptors dHNE **3** and HNE **1** (Figure 2) were first compared. Precise determination of second-order rates was not possible in this case because different sets of cysteine (Cys) residues on Keap1 reportedly interact with a given electrophile,[9,11] and presumably do so at different rates.[25] Under the conditions in which His_6-Keap1 was directly treated with 1 equiv of reactive LDE of interest (Figure 5), the data with

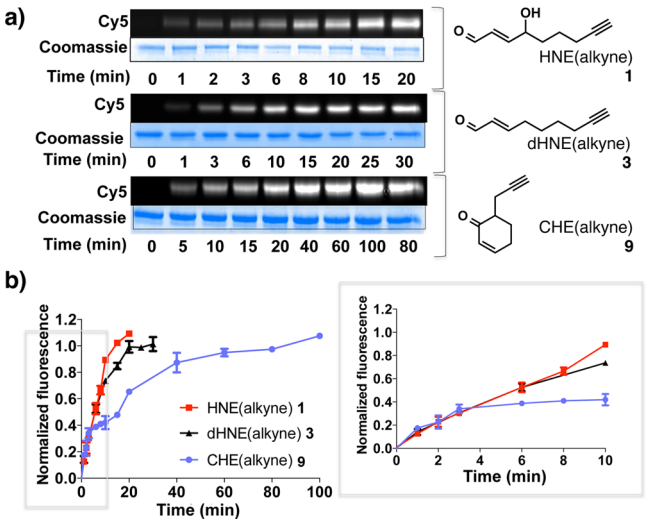

Figure 5. (a) Representative in-gel fluorescence data for the time-dependent alkylation of recombinant human His_6-Keap1 with **1**, **3**, and **9**. (b) Quantitation of the data in (a) (n = 2) as progress curve plots. Inset shows the first 10 min. The "normalized fluorescence" was derived by first calculating the ratio of Cy5: Coomassie signals for each time point, and normalizing the resultant values to the respective mean of the last three time points for each LDE.

dHNE **3** showed that it took approximately twice as long for the Cy5-signal intensity on Keap1 to reach saturation compared to HNE **1**. Notably, however, the initial (<10 min) rates of covalent adduction by **3** and **1** were comparable. The less reactive enone CHE **9** was next examined under identical conditions. The reaction profile was overall clearly distinct from those of dHNE **3** and HNE **1**. Alkylation with CHE **9** required a ∼4–5-fold longer time to reach Cy5-signal saturation on Keap1 (Figure 5b). However, the initial alkylation rate of CHE **9** was not significantly different from that of linear enals **1** or **3** (Figure 5b inset).

These data could be most simply explained by a two-step mechanism involving assembly of an encounter complex between Keap1 and the electrophile, followed by alkylation. In one possible mechanistic scheme (*A*), CHE **9** would have a

DOI: 10.1021/ja5132648
J. Am. Chem. Soc. 2015, 137, 6232–6244

lower affinity for Keap1 with respect to dHNE **3** which would have a lower affinity than HNE **1**. An alternative mechanism (*B*) is that CHE **9** interacts with fewer cysteines (Cys's) than dHNE **3** and HNE **1** during encounter complex formation. Thus, as alkylation progresses, the number of reactive sites on the protein is depleted, and hence the rate drops off. A hybrid of (*A*) and (*B*) also remains a possible mechanism.

Residue Availability and Specificity in Keap1 Alkylation. CHE **9** and HNE **1** featured distinct progress curves for their reactions with recombinant Keap1 in solution (Figure 5). As an initial step to probe the Keap1 Cys residue pools available to react with HNE **1** and CHE **9**, LC–MS/MS analysis was performed. Subsequent to direct treatment of recombinant Halo-Keap1 with 1 equiv of CHE **9**, LC–MS/MS analysis showed CHE-derived modifications on 2 Cys residues, C151 and C288, with respective Mascot ion scores (IS) of 48 and 36 (Table S3). Substituting HNE **1** in place of CHE **9** and replication of the experiment revealed 6 HNEylated residues instead—C77, C151, C226, C273, C319 and C368—with IS's 60, 74, 54, 61, 40 and 95, respectively.[13] The increased promiscuity of HNE relative to CHE thus most likely accounts for the differences in overall alkylation rate seen in the progress curves above (Figure 5b). In addition, C151 was identified as an overlap between the two sets of Cys residues characterized to be modified during CHE- as well as HNE-adduction events. It is worth noting that all these Cys residues are implicated in Keap1 electrophile response.[11e]

We also progressed to investigate whether T-REX versus nontargeted delivery shared similar Cys alkylation patterns on Keap1 with the use of respective caged precursors Ht-Pre-CHE **22** and Ht-Pre-HNE **17**. Under T-REX conditions in which the recombinant Halo-Keap1 in solution was targeted by CHE **9** using 1 equiv of Ht-Pre-CHE **22** and subsequent light exposure, C151 of Keap1 was the only residue modified (IS, 50) (Table S4 and S5). On the other hand, T-REX-targeted HNEylation with Ht-Pre-HNE **17** under identical conditions yielded 2 Cys residues HNEylated, C226 and C368 (IS, 51 and 61, respectively).[13] These data further corroborated the hypothesis of a lower number of Cys residues available for CHE **9** over HNE **1**.

T-REX Delivery in Cells. Upon the basis of the in vitro kinetic data, the caged precursors to LDEs constructed in our toolbox, including enones housing reduced intrinsic electrophilicity (Figure 2), should efficiently alkylate Keap1 in cells, provided the postulated encounter complex mechanism is operative. T-REX delivery was performed in HEK-293 cells stably expressing Halo-Keap1 fusion protein (Figure 6 and S2). The percentage delivery efficiency in cells was determined using eq 1 in which superscript "*x*" designates sample exposed to both light and TEV protease. Superscript "*y*" designates sample not treated with light or TEV. Briefly, the method involved quantitating the amount of Cy5 signal on Keap1 (post photoactivation and TEV-protease-catalyzed separation of Halo and Keap1 domains subsequent to cell lysis and Click coupling), relative to the signal on Halo-Keap1 in the sample not exposed to light and TEV. Western blot (WB) of Keap1 validated equal protein levels (see eq 1 and also Figure S2 legend). The remaining Cy5 signal on Halo, post TEV cleavage, results from incomplete release of the reactive electrophile from the cage, presumably due to lower photouncaging efficiency in cells.

The remaining signal on Halo band was accounted for in quantitating the delivery efficiency as shown in eq 1.

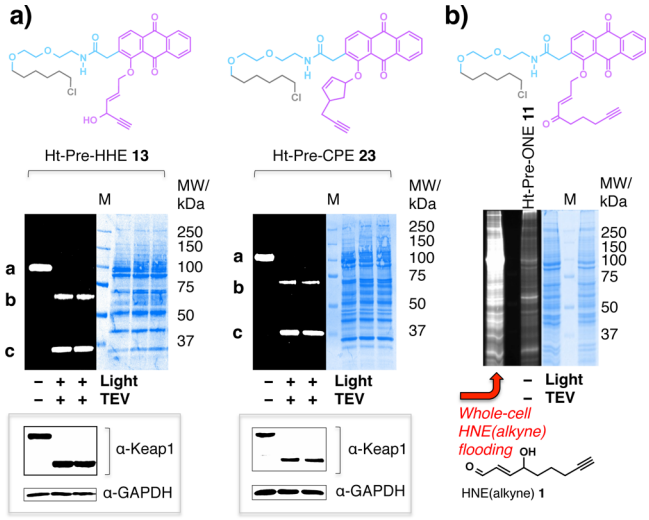

Figure 6. (a) Representative data for T-REX-assisted Keap1-specific electrophilic adduction (a) versus whole-cell electrophile flooding (b). (a) Live HEK-293 cells stably expressing Halo-Keap1 were treated with 25 μM **13** and **23**, and the excess washed out. After 20 min light exposure, cells were lysed, and the lysate was treated with TEV-protease (separating Halo and Keap1), followed by Cy5 click assay reagents. Band a, Halo–Keap1 (104 kDa), b, Keap1 (70 kDa, post TEV cleavage), c, Halo (33 kDa). Dark gel is the fluorescence gel of the Coomassie-stained PVDF membrane on the right. Independent duplicates are shown for light-activated TEV-treated samples. "M" indicates the ladder lane. Insets show western blot. See also Figure S2, Table 1, and eq 1. (b) Whole-cell HNE **1** (25 μM) treatment target nonspecifically. Ht-Pre-ONE **11** reacts before uncaging.

$$\left(\frac{Cy5_{Keap1}{}^{x}/WB_{Keap1}{}^{x}}{(Cy5_{Halo\text{-}Keap1}{}^{y} - Cy5_{Halo}{}^{x})/WB_{Halo\text{-}Keap1}{}^{y}}\right) \quad (1)$$

We observed that ONE **2** was ineffective because the caged precursor Ht-Pre-ONE **11** itself covalently conjugated to cellular proteins nonspecifically prior to photoliberation (Table 1, entry 2, and Figure 6b). This finding can be explained because Ht-Pre-ONE **11** itself harbors a reactive Michael acceptor enone moiety. This observation also underscores the fact that multiple target modifications are unavoidable from whole-cell soaking with highly reactive enals and enones such as HNE and ONE.[4] It is worth noting that despite overexpressing Halo-Keap1 in these cells, Halo-Keap1 did not even represent one of the bands displaying strongest Cy5 intensity (Figure 6b).

On the other hand, temporally controlled targeting of enals **2**–**5** to Keap1 was successful (Table 1, Figure 6a and S2) as in the previous proof-of-concept targeting of **1** to specific proteins in cells.[12] Within our limit of detection, the delivery was target-specific, a result in stark contrast to whole-cell electrophile flooding (Figure 6b and ref 4). Among all linear alkenals delivered (Table 1, entry 2–6), the electrophiles bearing a 4-hydroxy group (**4** and **5**) gave a slightly higher targeting (~30%) than the less electrophilic 4-dehydroxy-analog, dHNE **3** (21%), indicating that reactivity can play a part in dictating delivery efficiency, but it is not largely significant.

The length of the carbon chain did not appear to significantly impede the reactivity with Keap1 in cells since Ht-Pre-HHE **13** and Ht-Pre-HDE **14** provided similar levels of Keap1-targeted alkylation efficiency. The issue associated with the release of 16-carbon chain 2-HD **7** from **16** was discussed above (Figure S1).

DOI: 10.1021/ja5132648
J. Am. Chem. Soc. 2015, 137, 6232–6244

Table 1. Scope of T-REX Electrophile Toolbox

Entry	HaloTag-targetable caged precursor	Delivered reactive electrophiles (alkyne-functionalized)[a]		% Delivery efficiency in live cells[b]
1	Ht-Pre-HNE **17**	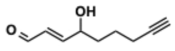	HNE(alkyne) **1**	33 ± 2
2	Ht-Pre-ONE **11**	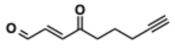	ONE(alkyne) **2**	–[c]
3	Ht-Pre-dHNE **12**	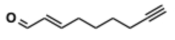	dHNE(alkyne) **3**	21 ± 2
4	Ht-Pre-HHE **13**	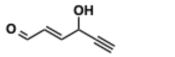	HHE(alkyne) **4**	30 ± 1
5	Ht-Pre-HDE **14**	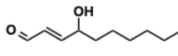	HDE(alkyne) **5**	29 ± 1
6	Ht-Pre-HDDE **15**	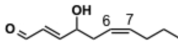	HDDE(alkyne) **6**	–[c]
7	Ht-Pre-2-HD **16**	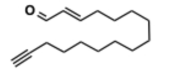	2-HD(alkyne) **7**	–[c]
8	Ht-Pre-DE **21**	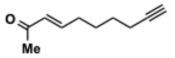	DE(alkyne) **8**	22 ± 2
9	Ht-Pre-CHE **22**	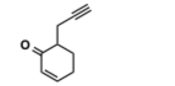	CHE(alkyne) **9**	25 ± 1
10	Ht-Pre-CPE **23**	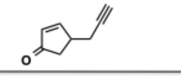	CPE(alkyne) **10**	19 ± 2

[a]Racemic where applicable. [b]Error range is SD (n = 6). See also Figure 6 and S2. [c]Not determined (see discussion in text).

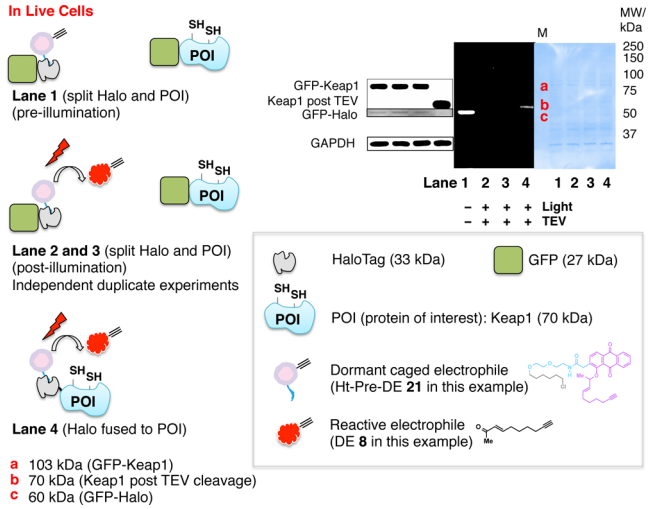

Figure 7. Mechanistic basis of T-REX platform supports proximity-induced reactivity concept within the "target–signal encounter complex". In-cell T-REX experiment in which Halo and Keap1 were not fused failed to deliver electrophile DE **8** to Keap1 using Ht-Pre-DE **21** and subsequent illumination (Lane 2 and 3, independent duplicates). By contrast, successful targeted delivery was achieved when Halo and Keap1 were fused (Lane 4 and also see Figre S2b). Schematic representations for each Lane are shown on the left. DE adduction of Keap1 (post TEV-protease cleavage) was observed (band b on gel) as expected in Lane 4. Western blot data and coomassie-stained PVDF were also shown. Bands a, b, and c correspond to GFP-Keap1 (103 kDa), Keap1 (70 kDa, post TEV-cleavage), and GFP-Halo (60 kDa), respectively. "M" indicates the ladder lane. Inset shows reference to the schematics. Rabbit polyclonal anti-GFP primary antibody (sc-8334) was used to probe GFP-Halo protein. All forms of proteins containing Keap1 were probed by mouse monoclonal anti-Keap1 primary antibody (Ab119403). See also Figure S3 and S4 for analogous data sets with non-GFP-fused Keap1.

The delivery with Ht-Pre-HDDE **15** however failed. We speculated that the unsuccessful T-REX-targeted delivery of HDDE **6** is likely due to intramolecular photoinduced side reaction between the *cis*-alkene at C6–C7 and the terminal alkyne, thereby destroying the reporter alkyne unit.[26] This proposal was supported by 29% delivery efficiency attainable with HDE **5** that has no C6–C7 alkene but is otherwise identical to HDDE **6**.

The delivery efficiency of linear enones was next investigated. The targeted delivery efficiency of DE **8** in cells using Ht-Pre-DE **21** gave 22% delivery, indicating that Keap1 is also susceptible to linear enones, with delivery efficiency similar to that of 4-dehydroxylated enal dHNE **3** (Table 1, entry 3 and 8). Directed alkylation with cyclic electrophile CHE **9** (derived from photouncaging of Ht-Pre-CHE **22**) resulted in 25% delivery efficiency. The delivery efficiency was in the same range as linear enals **1**–**5** and enone DE **8** (Table 1). Ht-Pre-CPE **23** that models simple cyclopentenones was also tested in cells. The 19% delivery efficiency for CPE **10** was on par with that of dHNE **3** and DE **8** (Figure 7 and S2). These data collectively imply that T-REX is a functional platform for selectively perturbing an intracellular signaling target with electronically disparate bioactive electrophiles. The similar levels of delivery efficiencies across all the small-molecule inducers tested show that T-REX has a broad substrate delivery scope that will enable quantitative profiling of many small-molecule electrophiles in the future, with target-specificity as well as temporal control.

T-REX Delivery Mechanism in Cells. We next proceeded to investigate the delivery mechanism of T-REX in live cells. Our current model predicts that fusion of the HaloTag to the target protein is required for T-REX delivery to occur. To test this postulate, two separate expression vectors encoding the two fusion genes, GFP-Halo and GFP-Keap1, were used to coexpress Halo and Keap1 separately in HEK-293 cells. These cells were subjected to T-REX conditions using Ht-Pre-DE **21** as an example (Figure 7). This condition showed no Cy5 signal on Keap1. Replicating these experiments with non-GFP-tagged constructs, i.e., coexpression of Halo protein and Keap1 proteins, also resulted in identical outcomes (Figure S3). Importantly, no background protein reactivity was observed either, indicating that nonspecific protein targeting is minimal under T-REX conditions, even when no target protein fused to HaloTag bearing the caged precursor is available. On the other hand, as we disclosed above (Figure S2c and Table 1), alkylation of Keap1 by DE **8** was reproducibly observed in the positive control experiment in which HaloTag was fused to Keap1 (Figure 7). We further validated this proximity-induced targeting concept by comparing the delivery efficiency of T-REX using Ht-Pre-HNE **17** in a system in which Halo and Keap1 were coexpressed separately, to that in which Halo and Keap1 were fused but otherwise performed under identical conditions. Keap1 failed to be effectively alkylated by HNE **1** when the HaloTag was expressed as a separate protein in cells (Figure S4). These data altogether support the directed alkylation model within the target–signal encounter complex.

DOI: 10.1021/ja5132648
J. Am. Chem. Soc. 2015, 137, 6232–6244

The proximity-induced targeted delivery model was further validated by the results from pathway activation studies described in the following sections.

Quantitating Relative Downstream Signaling Strength: The Degree of Nrf2 Stabilization. Our recent data show that Keap1-specific substoichiometric (~34%) HNEylation enabled by T-REX is sufficient to induce downstream response, blocking of Nrf2 proteasomal degradation and upregulation of ARE.[13] We here examined the extent to which modest chemical perturbations across the various LDE signals delivered selectively to Keap1 in cells modulate the relative levels of Nrf2–ARE activation. We accomplished this goal using two independent quantitative readouts: (1) western blot analysis probing the upregulation of Nrf2 steady-state levels, and (2) reporter gene assay quantitating the fold increment of ARE-driven firefly luciferase signal, normalized over constitutively expressed *Renilla* luciferase (Figure 8).

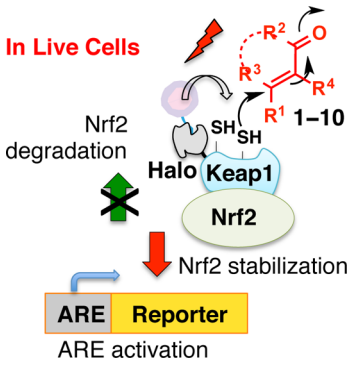

Figure 8. Two independent readouts for quantitating the downstream signaling strength selectively elicited by target- and signal-specific electrophilic modification of a specific upstream target in cells. T-REX-assisted temporally controlled Keap1-specific modifications resulted in blockage of Nrf2 degradation. Accumulating Nrf2 (assessed by western blot) consequently enabled ARE activation (assessed by ARE-luciferase assay).

HEK-293 cells expressing Halo-Keap1 and Nrf2 were treated with the designated caged precursor. As a proof-of-concept comparison, Ht-Pre-HNE **17**, Ht-Pre-dHNE **12**, Ht-Pre-DE **21**, Ht-Pre-CHE **22**, and Ht-Pre-CPE **23** were chosen because they reflect delivery of electronically as well as sterically discriminated electrophiles (long-chain enals HNE **1** and dHNE **3**, and cyclic/acyclic enones DE **8**, CHE **9**, and CPE **10**). As described above, the targeted delivery efficiencies to Keap1 quantitated using in-gel fluorescence analysis subsequent to Click coupling assays were comparable across the majority of these electrophiles, dHNE **3**, DE **8**, CHE **9**, and CPE **10** (19–25%), except ~33% for HNE **1** (Table 1 and Figure 6 and S2). Should Keap1 alkylation event determine the fate of downstream signaling, a similar extent of downstream signaling strength should be achievable. On the other hand, should Keap1 sense not only electrophile adduction, but also some aspect of the individual LDE signal, differing levels of ARE signaling would be expected depending on the LDE employed.

The degree of Nrf2 stabilization was first interrogated. Western blot analysis showed similar levels of upregulation (~2–3 fold) of Nrf2 protein expression across the representative electrophiles (Figure 9a and S5). Light-alone or caged-precursor-alone treatment did not lead to statistically significant Nrf2 stabilization (Figure 9c). As a comparison, we

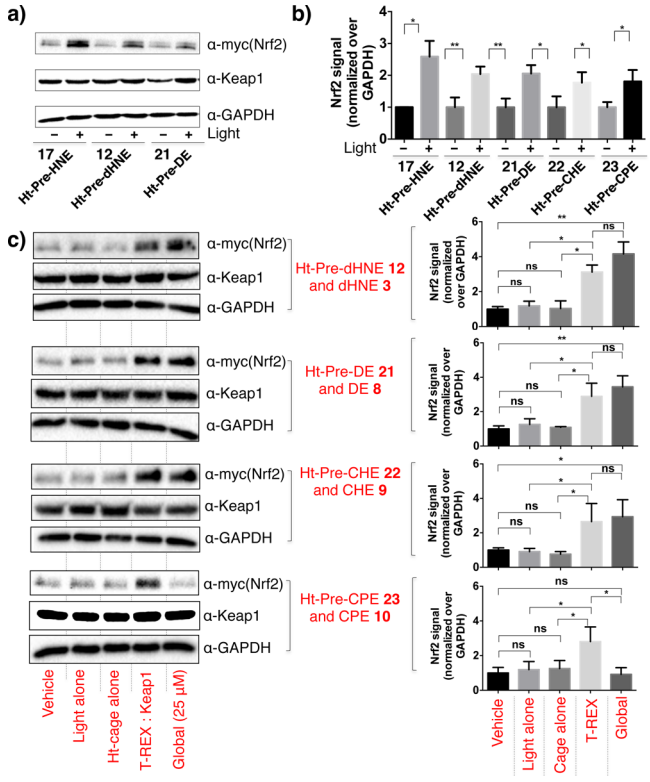

Figure 9. Upregulation of Nrf2 protein expression levels elicited by T-REX-assisted Keap1-specific electrophilic modification in HEK-293 cells expressing Halo-Keap1 and Nrf2. See also Figure S5. (a) Representative western blot data from T-REX conditions in comparison with Ht-caged precursor treatment alone (i.e., no light). (b) Quantitation of data in (a, c) and in Figure S5a–b. (c) Representative western blot data (left) and corresponding quantitation (right) from T-REX conditions in comparison with whole-cell electrophile (25 μM) soaking. Error bars designate SD over 3 independent biological replicates. Nrf2 levels were assessed after 18 h incubation period post 20 min light exposure. Vehicle, DMSO.

also analyzed the extent of phenotypic Nrf2 stabilization induced upon global electrophile stimulation. Twenty-five μM LDE was selected as the concentration of choice at which significant downstream response (assessed by ARE activation, Figure S6, vide infra) was attained while maintaining ~80–90% of cell viability (assessed by alamarBlue assay) (Figure S7). The western blot analysis showed that under identical incubation time and conditions, whole-cell electrophile incubation, using dHNE **3**, DE **8**, or CHE **9**, led to a similar degree of Nrf2 stabilization (Figure 9b and S5). Interestingly, the data showed the direct treatment of cyclopentenone CPE **10** did not result in Nrf2 stabilization. The basis behind this interesting distinction between T-REX-assisted targeted CPE delivery and whole-cell CPE **10** treatment is probed in the next section.

Quantitating Relative Downstream Signaling Strength: The Degree of ARE Upregulation. The magnitude of Nrf2-dependent ARE induction was next interrogated in HEK-293 cells ectopically expressing ARE-inducible firefly and constitutive *Renilla* luciferases alongside Halo-Keap1 and Nrf2 (Figure 10). The same set of caged precursors—Ht-Pre-HNE **17**, Ht-Pre-dHNE **12**, Ht-Pre-DE **21**, Ht-Pre-CHE **22**, and Ht-Pre-CPE **23**—used in evaluating the Nrf2 stabilization (Figure 9 and S5) was analyzed in evaluating ARE activation. Consistent with the similar delivery efficiency to Keap1, a comparable (~1.5–3-fold) enhancement

DOI: 10.1021/ja5132648
J. Am. Chem. Soc. 2015, 137, 6232–6244

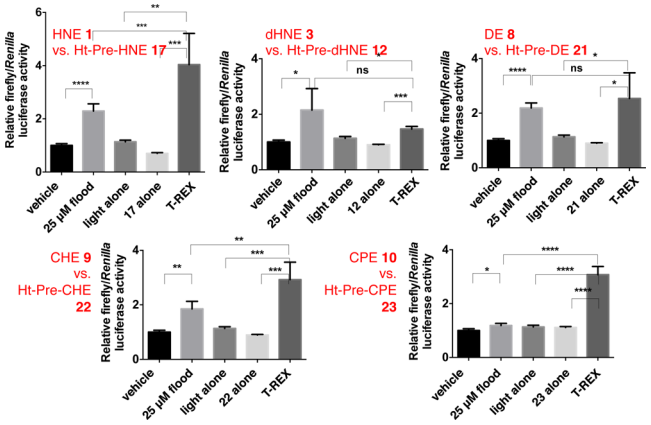

Figure 10. Reporter gene assay data on ARE upregulation in HEK-293 cells stably expressing Halo-Keap1 and transiently expressing Nrf2 alongside ARE-inducible firefly luciferase and constitutive *Renilla* luciferase. For each LDE, the magnitude of ARE induction is compared between T-REX conditions and whole-cell electrophile (25 μM) flooding. Vehicle, DMSO. See also Figure S6−S7 and S13 for titration of ARE response and cell viability analyses. Error bars designate SD over 3 independent biological replicates. The ARE response was analyzed after 18 h incubation period post 20 min light exposure.

of downstream ARE response was measured for each LDE with respect to vehicle controls (Figure 10b). The caged precursor alone or light alone controls showed no significant ARE upregulation. The relatively higher fold increase in ARE induction from Ht-Pre-HNE **17** and Ht-Pre-CHE **22** may be correlated with their delivery efficiencies to Keap1 lying at the higher end, ∼33 and ∼25%, respectively (Table 1, and Figure 6 and S2).

As with Nrf2 stabilization readout (Figure 9 and S5), we also analyzed the impact on ARE upregulation from whole-cell electrophile stimulation. Titration studies first showed that 25 μM LDE in these studies provided near-maximal levels of ARE induction (Figure S6) without compromising viability assessed at 18 h post treatment (Figure S7). As with our previous finding on HNEylation,[13] the level of ARE response from T-REX-targeted approach largely phenocopied that attainable from whole-cell treatment for all cases except CPE **10**. With global treatment of CPE **10**, we failed to observe both Nrf2 stabilization and ARE upregulation (Figure 9b−c and S5b−c), although CPE **10** is still able to deplete cell viability in a dose-dependent manner (Figure S7). At 25 μM, it is also able to penetrate cells and alkylate Keap1 within 1 h treatment (Figure S9) despite no measurable ARE upregulation. On the other hand, targeted approach clearly resulted in downstream signal amplification using both types of readouts (Figure 9, 10 and S5). To delve deeper into possible reasons behind the lack of ARE response from global CPE **10** stimulation under noncytotoxic conditions, dose-dependent titration was performed including an earlier time point (4 h) (Figure S10a). Although at 18 h time point, the ARE response failed to activate until cytotoxic concentrations of CPE **10** were applied (viability EC_{50} ∼ 103 μM, Figure S7), the ARE response was observable at the earlier (4 h) time point, albeit to a limited level. With the T-REX method that delivers CPE **10** specifically to Keap1 alone, strong ARE activation was achieved at 18 h post modification (Figure S10b). The time dependent off-target mixed responses stemming from whole-cell covalent modification by CPE **10** that accumulate during the multihit scenario may in part explain this interesting observation. The off-target spectra also likely differ among individual LDEs. T-REX-targeted approach may thus prove useful for promoting downstream signal amplification by its ability to perform precision targeting.

Blocking Pathway Activation in Applying T-REX on the Non-HaloTag-Fused System. Since we had shown that Keap1-specific targeting required the HaloTag to be genetically fused to Keap1, we postulated that if Halo and Keap1 were expressed separately [in which no LDE targeting occurred to Keap1 (Figure 7, S3, and S4)], no increase in Nrf2 steady-state levels would be observed under T-REX conditions. Consistent with this expectation, when HaloTag and Keap1 were co-overexpressed as two separate proteins, Nrf2 stabilization was abolished upon applying T-REX using Ht-Pre-HNE **17** and Ht-Pre-DE **21**, respectively (Figure S8). These results strongly imply that Nrf2 upregulation we observe under T-REX targeting with Halo-Keap1 (Figure 9 and S5) is solely due to Keap1-targeted modification. Moreover, since ARE activation occurs due to modification of sensor proteins (including Keap1), the lack of AR upregulation in the case where T-REX is performed in the system in which Halo and Keap1 are expressed separately[13] confirms our postulate that T-REX conditions do not perturb the cell.

Functional Redundancy of Cys Residues in Keap1-Specific Electrophilic Regulation. Our recent data with T-REX-assisted Keap1-targeted HNEylation in HEK-293 cells argue against the existence of obligatory Cys residues among the 27 Cys residues of human Keap1 protein that must be HNEylated to trigger pathway activation. To evaluate the extent to which residue specificity plays a general role in Keap1-specific electrophilic regulation, we identified Cys residues modified subsequent to treatment with CHE **9** either globally (25 μM, 20 min) or by using Ht-Pre-CHE **22** under T-REX conditions (Table S6 and S7). TALON enrichment of Halo-Keap1 protein from treated cells under native conditions, and subsequent trypsin digestion and LC−MS/MS analysis, revealed C613 (23, 0.005) and C489 (13, 0.05) as sites modified under T-REX conditions. The two numbers in parentheses designate Mascot ion scores and p-values, respectively. Because the Mascot scoring depends on the size of database used for the search and in our case the protein identity was known for Keap1, which we purified from HEK-293 cells, the low scores were expected. However, across all samples, either T-REX or global treatment, we set the Mascot ion score threshold to be the same with the p-value of ≤0.05 (see Supporting Information method section for details). This setting precluded the possibility of overlooking such low-score residues in other data sets. In our opinion, modification at C489 should be regarded as a low-confidence score with p-value of 0.05. This modification was thus not further considered in subsequent sections unless otherwise stated.

On the other hand, under whole-cell CHE **9** treatment, C513/C518 [75, (3.2×10^{-8})], and C273 [52, (6×10^{-6})] were modified. The numbers in square brackets represent Mascot ion scores and p-values, respectively. On the basis of the site analysis results of Mascot search, the chances of modification on C513 and C518 within the singly CHE-**9**-modified tryptic peptide were 28 and 72%, respectively. Our in vitro MS analysis above showed that C151 was modified using T-REX on recombinant Halo-Keap1. Differences in the identitiy of residues modified may be due to different Keap1 conformational states in cellular environment, a result

DOI: 10.1021/ja5132648
J. Am. Chem. Soc. 2015, 137, 6232−6244

consistent with our recent analysis of residue specificity in HNEylation.[13]

As a means to examine functional importance of the two specific residues modified under T-REX conditions in cells, mutagenesis studies were performed (Table S3). Although the modification at C489 represents a low-confidence score (vide supra), we chose to include this residue in our functional mutagenesis studies for completeness sake. We found that the single mutants (C613S, and C489S), as well as the double mutant (C613S/C489S) were still alkylated by CHE **9** in cells during T-REX targeting (Figure S11a). Although the basal levels of ARE are affected by mutation, the mutants remained largely responsive to targeted electrophilic modification by CHE **9** with efficiencies similar to wild type, both in terms of stabilizing Nrf2 protein (Figure S11b) and in ARE activation (Figure S11c). Furthermore, the fact that under noninduced conditions, mutation of C613 and C489 affected the unstimulated steady-state levels of Nrf2 (Figure S11c) indicates that these residues are important for Keap1 funcitonal integrity. This statment is supported by our previous work and that of others examining the consequences of point mutations at C151 and C288; C151S/C288S also affects unstimulated Nrf2 levels,[11b,h,13] and the mutants are still HNEylated upon T-REX targeting.[13] Accordingly, there is no reason to assume that alkylation of the newly found CHE **9**-modified residues in the present study, C613 and C489, would not affect Nrf2 steady-state levels. Indeed, both C613 and C489 of recombinant human Keap1 have reportedly been modified by overlapping sets of electrophiles in vitro.[11e] Our data showed that C613S and C489S mutants are able to respond to CHE **9** under T-REX targeted conditions (Figure S11b and S11c), thereby indicating that other residues on Keap1 are also CHE **9**-sensitive in cells. These data are altogether consistent with our conclusions elsewhere within this present study or in previous work.[13]

Evaluating the Extent of Keap1 LDE Modifcations under T-REX Conditions in Comparison with Whole-Cell LDE Flooding. *Gel-Based Analysis.* Using T-REX in cells, ~25% delivery efficiency of CHE **9** was achieved (Table 1 entry 9, and Figure S 2d). As shown in eq 1, the calculation of this ~25% delivery efficiency took into consideration the remaining caged precursor Ht-Pre-CHE **22** on Halo post 20 min light exposure in cells (approximately 1/4th of total caged precursor molecules remained on Halo post illumination due to incomplete uncaging in cells under the low-energy light conditions, Figure S 2d). Therefore, the percentage of Keap1 molecules modified by CHE **9** under T-REX conditions was ~19% (i.e., 25% × 3/4th). To estimate the percentage of Keap1 molecules modified under whole-cell LDE stimulation, we designed the following experiment. One set of cells ectopically expressing Halo-Keap1 was treated with Ht-Pre-CHE **22**. The Cy5 signal from this sample post cell lysis and Click coupling conditions provided us with the reference signal intensity that equates to one equivalent of CHE **9** stoichiometrically labeled to Halo-Keap1 fusion protein. This reference point is made possible because 1:1 covalent binding between HaloTag and the caged precursor molecule is achieved under our experimental conditions.[12] To another set of cells ectopically expressing Halo-Keap1, direct CHE **9** treatment (25 μM, 20 min) followed by cell lysis, Click coupling, and in-gel fluorescence analysis was applied. Comparison between the Cy5 signal intensities between these two samples showed the extent of LDE labeling under global conditions was ~1.2-fold higher than if Keap1 were to be labled stoichiometrically (Figure 11). Importantly, this observation implies that the total

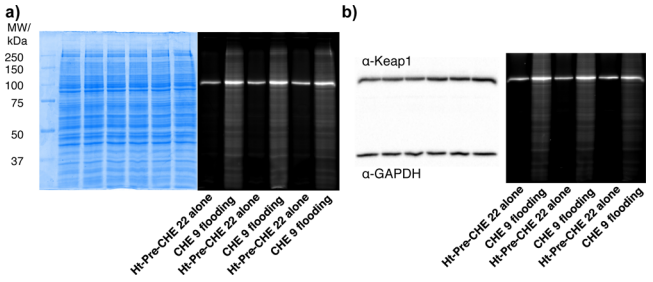

Figure 11. Representative data from in-gel fluorescence analysis evaluating the extent of Keap1 modifications under whole-cell LDE flooding. Signal from samples designated as "Ht-Pre-CHE **22** alone" equates to 1 equiv of CHE-alkyne **9** stoichiometrically labeled to Halo-Keap1. See discussion in text. The data in each case originate from three independent biological replicates. (a) "Ht-Pre-CHE **22** alone" designates live HEK-293 cells transiently expressing Halo-Keap1 treated with Ht-Pre-CHE **22** alone without exposure to light (see SI for details), followed by cell lysis and Click coupling to Cy5 azide. "CHE **9** flooding" designates whole-cell CHE **9** treatment (25 μM, 20 min), followed by cell lysis and Click coupling with Cy5 azide. The corresponding Coomassie stained gel is shown on the left. (b) Remaining lysate samples from experiment in (a) were subjected to Click coupling for in-gel fluorescence analysis followed by western blot using antibodies to Keap1 and GAPDH (loading control). See also Figure S2d.

amount of CHE **9** reacted with Keap1 under whole-cell flooding conditions (25 μM CHE **9**, 20 min) is ~6-fold higher that that achieved under T-REX conditions (Figure S2d), and yet the former method provides no additional benefit in terms of antioxidant response pathway activation (Figure 9, 10, and S5).

MS-Based Analysis. We also further analyzed the LC−MS/MS data of CHE **9** modifications in cells under T-REX and global treatment. The crude estimations of the extents of modifications were made using the peak integration method. Briefly, ions (m/z) corresponding to the CHE **9**-modified peptides and the corresponding nonmodified peptides were extracted from total-ion chromatograms (TICs) and the peaks were integrated using Analyst 1.1 and normalized to the total area under the peaks representing the modified and the nonmodified peptides. The percentage modifications were 15% for C613 (under T-REX), and 3% for C513/C518, and 2% for C273 (under whole-cell CHE **9** flooding).

Data Interpretations and Implications. Notably, upon comparing these two independent procedures (i.e., in-gel fluorescence analysis and ion peak integration method), the percentage Keap1 modified (15%) for the C613 residue under T-REX conditions was within the range of ~19% modification derived from in-gel-fluorescence-based analysis discussed above. This observation implies that under T-REX conditions, a significant fraction of the released enone was delivered to one particular Cys residue (C613), and that no significant loss of CHE modification occurred under analytical conditions. However, since our downstream pathway analysis and functional mutagenesis studies showed that the magnitude of pathway activation by T-REX method was not dependent upon this specific Cys (Figure S11), the results suggest that other Cys residues within Keap1 can compensate for the lack of C613, a result that is consistent with functional redundancy displayed

DOI: 10.1021/ja5132648
J. Am. Chem. Soc. 2015, 137, 6232−6244

by multiple Cys residues discussed elsewhere in this manuscript.

Under whole-cell CHE **9** stimulation, the ion peak integration method detected only two residues modified (C513/518, and C273) and both within 2−3% modifications. Our simplest interpretation for the low percentage modifications is that because Keap1 is a promiscuous sensor, the model predicts all Cys residues of Keap1 are likely available to react with a reactive LDE present in excess. Indeed, various reports have collectively shown that 26 Cys's out of 27 Cys residues-bearing human Keap1 are modified upon global exposure to a range of reactive electrophiles.[11] Thus, under whole-cell flooding, average percentage of Keap1 molecules modified that we deduced from in-gel fluorescence assay data would be 4.4% (i.e., 120%/27) since the labeling is 1.2-fold (or 120%) of the reference Cy5 signal intensity (Figure 11). The 4.4% was largely similar to the 2−3% modifications calculated from peak integration above for the modifications at C513/518 and C273 under global CHE **9** treatment. Given such a low modification percentage, the chemical complexity of LDE modification of Cys's and the number of possible adducts, many of the Cys's modified under global LDE flooding conditions are likely below the limit of detection. The residues that were detected could be marginally more kinetically competent than other Cys's, form adducts with higher stability to analytical processing, yield peptides with greater ionization properties, or simply more readily detectable above background noise. Although integrated ionization values are subject to various biases due to differential ionization properties of the modified versus unmodified fragments, the agreement of these results with our previous results and our newest observations in this work suggests that the confidence of our interpretations is reasonably high.

DISCUSSION

Gleaning a quantitative understanding of how cell signaling pathways function to deliver the most robust physiologic responses remains attractive for developing targeted therapies,[27a] engineering new signaling circuits,[27b] and establishing new biochemical regulatory paradigms.[27c] One of the major hurdles in modern cellular biochemisry is to map how specific chemical signal inputs, such as covalent protein modification of an intracellular signaling target, are directly linked to specific biologic signal outputs, such as transcriptional response.[28] In the field of redox-dependent cell signaling, these challenges are significant because (1) redox-mediator signals are highly reactive and diffusible and once exposed to the entire cell are able to modify multiple signaling targets simultaneously;[4a,c] (2) unlike conventional protein modifications that act as chemical signals, such as glycosylation, and phosphorylation, redox-linked modifications largely occur without enzyme assistance; and (3) unlike typical small-molecule covalent modifiers such as phosphoryl donors and glycans, the diffusible small-molecule redox-modulator signals are intrinsically highly reactive and cause stress-related cellular damage when generated uncontrollably.[1,3,7]

Our laboratory has recently introduced a new idea of redox-linked chemical perturbations that can be executed in a target-protein-specific and temporally controlled manner in living cells,[12] thereby eliminating multisensing−multiresponse outputs, such as oxidative stress-related phenotypes. Beyond the initial proof of concept demonstrated with a well-known endogenous chemical signal inducer (HNE **1**),[13] the scope, mechanistic basis, and generality of the new chemical biology platform, termed "targetable reactive electrophiles and oxidants", or T-REX, were unknown. In this manuscript, we addressed all of these concerns. Furthermore, we transformed the newly introduced T-REX idea into a generalizable platform with which we can gain important mechanistic insights into how the inducers of different chemical structure and reactivity influence the magnitude of target-specific signal amplification downstream.

The in vitro kinetic experiments on time-dependent alkylation of recombinant human Keap1 with three structurally and electronically discrete electrophiles HNE **1**, dHNE **3** and CHE **9** showed that although the progress curves were overall different, the initial alkylation rates were similar (Figure 5). Subsequent interrogations into the identity of Keap1 Cys residues modified by the different electrophiles showed that HNE **1** labeled many more cysteines than CHE **9**. These data together are most consistent with Keap1 having a similar maximal rate of alkylation with many different electrophiles but the number of Cys's able to interact productively is different for different electrophiles. Such a model would account for the difference in alkylation progress curves observed for HNE **1** versus CHE **9** because as the reaction progressed the reactive sites would be relatively constant for HNE **1** (promiscuous modifier) but would diminish for CHE **9** (a more specific modifier).

Subsequent assessment of T-REX-assisted LDE delivery efficiencies to Keap1 in cells showed that across various enals and enones featuring diverse small-molecule electrophilicity and conformational preference, the delivery efficiencies remained largely comparable (Table 1, Figure 6 and S2). Given the percentage of labeling we observed, significant differences in the extent of modifications between CHE **9** and more reactive enones would be expected unless an encounter complex was formed post photoliberation. Indeed, the fact that the delivery efficiency of 4-dehydroxy enal dHNE **3** to Keap1 in cells was not appreciably different from 4-hydroxylated variants (**1**, **4**−**6**), further supports that T-REX capacity on targeting LDEs to Keap1 in cells was not largely influenced by intrinsic electrophilicity of the reactive signals. This result was also expected based on the outcome of the in vitro kinetic analysis, which showed similar initial rates of alkylation across HNE **1**, dHNE **3**, and CHE **9** (Figure 5). Taken together, replicating T-REX under nontargetable conditions in which Halo and Keap1 proteins were separately expressed also showed no detectable alkylation of Keap1 in cells (Figure 7, S3, and S4), an outcome consistent with the formation of an initial encounter complex model. Any electrophilic signals diffusing beyond the Keap1 microenvironment are most likely captured by GSH present in high (~10 mM) concentrations.[24]

Lipid-derived Michael acceptor electrophiles constitute an important class of reactive small-molecule cues in redox-linked signal transduction.[1,3,4] The most recent decade has witnessed mounting evidence that linear enals/enones and prostaglandins regulate cytoprotective responses through covalent modifications of specific sensor proteins.[1,3,4,8,21] Synthetic Michael acceptor pharmacophores such as CDDOs[5c,d] and BG-12[5a,b] have also recently gained popularity for their therapeutic benefit in upregulating drug-relevant response such as Nrf2−ARE signaling. Although Keap1 modification is one of the principal mechanisms by which Nrf2−ARE axis is activated (Figure 8),[9−11] quantitating the extent of modifications—especially establishing linkage between the upstream target- and signal-specific alkylation to the degree of downstream signaling—is

DOI: 10.1021/ja5132648
J. Am. Chem. Soc. 2015, 137, 6232−6244

not possible under whole-cell LDE flooding. For instance, > 700 cysteines have been profiled as HNE-sensitive targets among ~1000 cysteines assayed from soluble fractions of HNE-treated human proteomes.[4a] Importantly, it has also been unclear whether modest structural variations within small-molecule inducers significantly perturb the downstream ARE-driven gene activation.[1c,4a] Previous structure−activity relationship studies of limited classes of Nrf2−ARE inducers have led to nonharmonious conclusions presumably because many of these reactive diffusible inducers also modify multiple redox-sensitive targets beyond Keap1.[11,14,15] Although permeability and stability, among other factors, may also play roles in muddying the waters, many of the upstream Nrf2 regulators, such as PKC, PI3K, ERK, p38 MAPK, PERK, etc., are also reportedly redox-sensitive in addition to Keap1 and thought to play complex roles in executing Nrf2−ARE response (Figure 2, inset).[10,11a,e] Thus, interpretation of the data in the realms of redox-dependent signaling derived from global small-molecule inducer treatment necessitates utmost caution.

Our recent pilot study discovered that T-REX-assisted targeted HNEylation on Keap1 alone is able to recapitulate Nrf2 stabilization and ARE upregulation achieved by whole-cell HNE bathing.[13] Our current data with Ht-Pre-dHNE **12**, Ht-Pre-DE **21**, Ht-Pre-CHE **22**, and Ht-Pre-CPE **23** (Table 1, and Figure 6 and S2) substantiate the previous finding. The virtually indistinguishable extent of Nrf2 upregulation (Figure 9 and S5) and ARE activation (Figure 10) that we now observed from alkylating Keap1 with different Michael acceptors of varied chemical properties gave us a second level of insights into the Keap1-selective electrophile response mechanisms. The comparable delivery efficiencies we quantitated above (Table 1) alongside the Nrf2−ARE upregulation data (Figure 8 and S5) together imply that the downstream response is likely controlled by alkylation events instead of specific LDE identity. Although Keap1 reacts with diverse LDEs at different overall rates, different overall reaction progress curves observed across three distinct LDEs (Figure 5), our cell-based data involving targeted delivery of a structurally diverse array of LDEs demonstrates that Keap1 will respond similarly to a similar modest level of modifications that importantly results in similar magnitudes of pathway activation. These data imply that Keap1 is remarkably insensitive to steric and electronic perturbations over a broad range of Michael acceptor inducers studied. The results strongly indicate that Keap1 has broad-ranging electrophile sensing ability. Such data presumably reflect the role of Keap1 as a guardian of the cell that has evolved to respond to various reactive stimuli,[14b] and suggest that Keap1 is thus optimally tuned for its complex physiologic sensing role of various LDEs.

Interestingly, in the case of CPE **10**, comparison with global electrophile flooding showed that T-REX is able to prompt signaling response, whereas multihit scenarios from whole-cell CPE **10** treatment did not afford measurable Nrf2−ARE response under otherwise identical conditions (Figure 9b−c and S5b−c). This observation was in spite of the fact that CPE **10** was still able to cause cytotoxicity from whole-cell treatement (Figure S7) and able to permeate and alkylate Keap1 (Figure S9) within 1 h treatment period. The minimal response observed at 4 h was nullified at 18 h (Figure S10a). Given the promiscuous nature of cyclopentenone-based LDEs including CPE **10**, we interpret this result to indicate that off-target effects are able to suppress the modest ARE activation observed initially. This interpretation is also backed up the fact that the magnitude of T-REX-assisted ARE upregulation for all LDEs studied is at least as high, and in the case of HNE **1**, CHE **9**, and CPE **10**, higher than the whole-cell LDE flooding. We conclude that targeted drug design toward Keap1-specific small-molecule modifiers may prove fruitful in activating the therapeutically beneficial Nrf2−ARE signaling axis, while circumventing nondesirable off-target modifications and associated cytoxicity. Interestingly, it is striking that global treatment with LDE such as CHE **9** leads to such a large excess of CHE **9** modification of Keap1 over T-REX conditions (~6 fold) (Figure 11 and S 2d), and yet there is no added bonus in activating Nrf2−ARE (Figure 9, 10, and S5). This result further testifies to the fact that global treatment conditions, although useful representatives of oxidative stress, are unlikely to recapitulate endogenous signaling processes well. Instead, uncontrolled bolus dosing likely leads to unintended conseqeunces that cannot be easily parsed.

Three independent sets of evidence give credence to the fact that our results are not due to artifacts of protein over-expression. (1) Targeted alkylation and pathway activation capabilities were both ablated in the nonfused system in which HaloTag and Keap1 were both overexpressed, but separately (Figure 7, S3, S4, and S8). (2) The magnitudes of whole-cell stimulated ARE upregulation were the same between native cells and cells overexpressing target proteins of interest (Figure S12). (3) Ht-Pre-ONE **11** bearing reactive enone labeled the entire lysate, yet the Halo-Keap1 was not the band with the highest intensity (Figure 6b).

In summary, T-REX approach recapitulates perturbation of a single signaling target with an array of reactive electrophiles in basal concentrations against the backdrop of an unperturbed proteome. In this way, the method enables the functional mapping of a specific chemical signal input on specific intracellular targets to the magnitude of signaling output. Our initial pilot tests on targeted HNEylation in cells show the generality with respect to two different targets of differential redox sensitivity, Keap1 and PTEN proteins,[12] and capability of single-target HNEylation in low-stoichiometry in eliciting physiologic response.[13] The study here (1) established a broader conceptual framework underlying T-REX targeted delivery concept, (2) shed initial mechanistic insights into the basis of the unique T-REX chemical biology method, and (3) highlighted a generalizable T-REX toolbox with which we can quantitatively link the upstream target- and signal-specific redox-linked perturbations to the strength of pathway activation. The proof of concept was exemplified using the validated drug target Nrf2−ARE pathway. When juxtaposed with the conventional whole-cell electrophile flooding that led to nonspecific alkylation (Figure 6b), T-REX strategy, which allows delivery efficiency to be quantitated, is likely a better representative of the responsiveness of individual signaling targets to specific modifications in their discrete cellular microenvironments in which hydrogen-bonding interactions, and the redox status, etc., at a given instant remain largely unperturbed.

It could be argued that for instance, the position of the HaloTag and resulting conformation of the fusion protein may bias T-REX to modify select Cys residues that are less frequently alkylated by LDE than in the endogenous signaling settings. However, similar levels of responses achieved between T-REX and whole-cell stimulation indicate that T-REX is able to elicit physiologically relevant signaling that unlikely stems from targeted modifications of nonfunctionally relevant

DOI: 10.1021/ja5132648
J. Am. Chem. Soc. 2015, 137, 6232−6244

cysteines. In the specific case with human Keap1, there is clearly a large degree of functional redundancy within the 27 Cys residues in eliciting electrophile signaling. The fact that HaloTagging is noninvasive to Keap1 functional properties,[13] subcellular localization patterns,[12] and Nrf2 binding[13] further attest to the unimpeding nature of HaloTagging and make T-REX a powerful tool to mimic endogenous LDE modifications on demand. Although polypharmacological benefits of small molecules are appreciated,[29] this model is unlikely applicable to reactive species such as HNE which irreversibly modifies >700 targets in soluble cellular fractions alone.[4a] Given this level of complexity, it is inherently challenging to quantitatively dissect the consequences of each physiologic modification event. T-REX occupies a privileged niche in this regard.

The caged precursors in T-REX were also noncytoxic (Figure S13). By contrast, global treatment with reactive LDEs depletes cell viability as expected (Figure S7). The ability to forge a mechanistic link between chemical-signal-specific modifications upstream and target-specific signal propagation downstream had not been easily attainable using whole-cell electrophile flooding approaches that are nondiscriminate, thereby (de)-activating many pathways simultaneously, or nullifying some phenotypic signaling responses. The generalizable T-REX-targeted delivery idea presents new opportunities toward quantitative understanding of the functional consequences of modest modifications on specific intracellular signaling targets. New levels of fundamental insights into individual LDE-specific signaling provide a deeper perspective on how these redox-linked signaling subsystems execute their optimum physiologic responses in cells.

■ ASSOCIATED CONTENT

Supporting Information

Synthesis procedures and characterization of caged precursors and intermediates, biochemical and cell-based assays, and supporting figures (Figure S1–S13), schemes (Scheme S1–S10), and tables (Table S1–S9). The Supporting Information is available free of charge on the ACS Publications website at DOI: 10.1021/ja5132648.

■ AUTHOR INFORMATION

Corresponding Author

*ya222@cornell.edu

Notes

The authors declare no competing financial interest.

■ ACKNOWLEDGMENTS

We thank Dr. Jiayang Li for assistance with cloning and LC–MS/MS sample preparations; Dr. Marcus J. C. Long for generating stably transfected cell lines; and Mrs. Saba Parvez and Steve Pisano for constructing the pMIR bicistronic expression plasmids encoding DsRed-(IRES)-His$_6$-Keap1 and DsRed-(IRES)-His$_6$-Halo–Keap1-C613S/C489S-mutants, respectively. We are grateful to Dr. Mike Fenwick of Prof. Ealick's laboratory for generating the Ht-Pre-CHE **22**-bound Halo model (Figure 1b); Dr. Sheng Zhang, Cornell Univeristy Proteomics Facility, for LC–MS/MS technical support on the samples with recombinant protein; and the laboratory of Prof. Hening Lin for the use of a LC–MS instrument. This research was supported by an NSF CAREER Award (CHE-1351400) and the Beckman Young Investigator Award (to Y.A.). Instrumentation used in this research was supported by an NIH Director's New Innovator Award (1DP2GM114850) (to Y.A.). J.A.H acknowledges the CBI training grant (T32GM008500, PI – Prof. Hening Lin). M.T.D. thanks the National Merit Scholarship Corporation for undergraduate study support at Cornell.

■ REFERENCES

(1) (a) In *Redox Signaling and Regulation in Biology and Medicine*; Jacob, C., Winyard, P. G., Eds.; Wiley-VCH: Weinheim, 2009. (b) Rudolph, T. K.; Freeman, B. A. *Sci. Signaling* **2009**, *2*, re7. (c) Jacobs, A. T.; Marnett, L. J. *Acc. Chem. Res.* **2010**, *43*, 673–683.

(2) (a) Walsh, C. T. In *Posttranslational Modification of Proteins: Expanding Nature's Inventory*; Roberts & Co.: Greenwood Village, CO, 2005. (b) Tarrant, M. K.; Cole, P. A. *Annu. Rev. Biochem.* **2009**, *78*, 797–825.

(3) (a) Schopfer, F. J.; Cipollina, C.; Freeman, B. A. *Chem. Rev.* **2011**, *111*, 5997–6021. (b) Fritz, K. Z.; Petersen, D. R. *Free Radical Biol. Med.* **2013**, *59*, 85–91.

(4) (a) Wang, C.; Weerapana, E.; Blewett, M. M.; Cravatt, B. F. *Nat. Methods* **2014**, *11*, 79–85. (b) Condreanu, S. G.; Zhang, B.; Sobecki, S. M.; Billheimer, D. D.; Liebler, D. C. *Mol. Cell. Proteomics* **2009**, *8*, 670–680. (c) Yang, J.; Tallman, K. A.; Porter, N. A.; Liebler, D. C. *Anal. Chem.* **2015**, *87*, 2535–2541.

(5) (a) Ruggieri, S.; Tortorella, C.; Gasperini, C. *Ther. Clin. Risk Manage.* **2014**, *10*, 229–239. (b) Phillips, J. T.; Fox, R. J. *Semin. Neurol.* **2013**, *33*, 56–65. (c) Liby, K. T.; Sporn, M. B. *Pharmacol. Rev.* **2012**, *64*, 972–1003. (d) Crunkhorn, S. *Nat. Rev. Drug Discovery* **2012**, *11*, 96. (e) Liby, K. T.; Yore, M. M.; Sporn, M. B. *Nat. Rev. Cancer* **2007**, *7*, 357–369.

(6) See, for example: (a) Long, E. K.; Picklo, M. J., Sr. *Free Radical Biol. Med.* **2010**, *49*, 1–8. (b) Riahi, Y.; Cohen, G.; Shamni, O.; Sasson, S. *Am. J. Physiol.: Endocrinol. Metab.* **2010**, *299*, E879–E886. (c) Chipuk, J. E.; McStay, G. P.; Bharti, A.; Kuwana, T.; Clarke, C. J.; Siskind, L. J.; Obeid, L. M.; Green, D. R. *Cell* **2012**, *148*, 988–1000. (d) Shibata, T.; Iio, K.; Kawai, Y.; Shibata, N.; Kawaguchi, M.; Toi, S.; Kobayashi, M.; Kobayashi, M.; Yamamoto, K.; Uchida, K. *J. Biol. Chem.* **2006**, *281*, 1196–1204. (e) Galligan, J. J.; Rose, K. L.; Beavers, N.; Hill, S.; Tallman, K. A.; Tansey, W. P.; Marnett, L. J. *J. Am. Chem. Soc.* **2014**, *136*, 11864–11866.

(7) (a) Leonard, S. E.; Carroll, K. S. *Curr. Opin. Chem. Biol.* **2011**, *15*, 88–102. (b) Winterbourn, C. C.; Hampton, M. B. *Free Radical Biol. Med.* **2008**, *45*, 549–561.

(8) Breyer, R. M.; Bagdassarian, C. K.; Myers, S. A.; Breyer, M. D. *Annu. Rev. Pharmacol. Toxicol.* **2001**, *41*, 661–690.

(9) (a) Hayes, J. D.; Dinkova-Kostova, A. T. *Trends Biochem. Sci.* **2014**, *39*, 199–218. (b) Ma, Q. *Annu. Rev. Pharmacol. Toxicol.* **2013**, *53*, 401–426.

(10) (a) He, X.; Ma, Q. *Mol. Pharmacol.* **2009**, *76*, 1265–1278. (b) Huang, Y.; Li, W.; Kong, A.-N. *Cell Biosci.* **2012**, *2*, 40. (c) Leonarduzzi, G.; Robbesyn, F.; Poli, G. *Free Radical Biol. Med.* **2004**, *11*, 1694–1702. (d) Numazawa, S.; Ishikawa, M.; Yoshida, A.; Tanaka, S.; Yoshida, T. *Am. J. Physiol.: Cell Physiol.* **2003**, *285*, C334–C342. (e) Castello, L.; Marengo, B.; Poli, G.; Chiarpotto, E. *Biochim. Biophys. Acta* **2005**, *1737*, 83–93. (f) Dozza, B.; Smith, M. A.; Perry, G.; Tabaton, M.; Strocchi, P. *J. Neurochem.* **2004**, *89*, 1224–1232. (g) Shearn, C. T.; Smathers, R. L.; Backos, D. S.; Reigan, P.; Orlicky, D. J.; Petersen, D. R. *Free Radical Biol. Med.* **2013**, *65*, 680–692.

(11) (a) Hur, W.; Gray, N. S. *Curr. Opin. Chem. Biol.* **2011**, *15*, 162–173. (b) Dinkova-Kostova, A. T. *Scientifica* **2012**, *2012*, 606104. (c) Kensler, T. W.; Wakabayashi, N.; Biswal, S. *Annu. Rev. Pharmacol. Toxicol.* **2007**, *47*, 89–116. (d) Motohashi, H.; Yamamoto, M. *Trends. Mol. Med.* **2004**, *10*, 549–557. (e) Bryan, H. K.; Olayanju, A.; Goldring, C. E.; Park, B. K. *Biochem. Pharmacol.* **2013**, *85*, 705–717. (f) Nguyen, T.; Nioi, P.; Pickett, C. B. *J. Biol. Chem.* **2009**, *284*, 13291–13295. (g) Takaya, K.; Suzuki, T.; Motohashi, H.; Onodera, K.; Satomi, S.; Kensler, T. W.; Yamamoto, M. *Free Radical Biol. Med.* **2012**, *53*, 817–827. (h) Zhang, D. D. *Drug Metab. Rev.* **2006**, *38*, 769–789.

DOI: 10.1021/ja5132648
J. Am. Chem. Soc. 2015, 137, 6232–6244

(12) Fang, X.; Fu, Y.; Long, M. J. C. L.; Haegele, J. H.; Ge, E. J.; Parvez, S.; Aye, Y. *J. Am. Chem. Soc.* **2013**, *135*, 14496−14499.
(13) Parvez, S.; Fu, Y.; Li, J.; Long, M. J. C.; Lin, H.-Y.; Lee, D. K.; Hu, G. S.; Aye, Y. *J. Am. Chem. Soc.* **2015**, *137*, 10−13.
(14) (a) Dinkova-Kostova, A. T.; Fahey, J. W.; Talalay, P. *Methods Enzymol.* **2004**, *382*, 423−448. (b) Ahn, Y.-H.; Hwang, Y.; Liu, H.; Wang, X. J.; Zhang, Y.; Stephenson, K. K.; Boronina, T. N.; Cole, R. N.; Dinkova-Kostova, A. T.; Talalay, P.; Cole, P. A. *Proc. Natl. Acad. Sci. U. S. A.* **2010**, *107*, 9590−9595.
(15) (a) Sporn, M. B.; Liby, K. T.; Yore, M. M.; Fu, L.; Lopchuk, J. M.; Gribble, G. W. *J. Nat. Prod.* **2011**, *74*, 537−545. (b) Dinkova-Kostova, A. T.; Talalay, P.; Sharkey, J.; Zhang, Y.; Holtzclaw, W. D.; Wang, X. J.; David, E.; Schiavoni, K. H.; Finlayson, S.; Mierke, D. F.; Honda, T. *J. Biol. Chem.* **2010**, *285*, 33747−33755. (c) Dinkova-Kostova, A. T.; Liby, K. T.; Stephenson, K. K.; Holtzclaw, W. D.; Gao, X.; Suh, N.; Williams, C.; Risingsong, R.; Honda, T.; Gribble, G. W.; Sporn, M. B.; Talalay, P. *Proc. Natl. Acad. Sci. U. S. A.* **2005**, *102*, 4584−4589. (d) Dinkova-Kostova, A. T.; Massiah, M. A.; Bozak, R. E.; Hicks, R. J.; Talalay, P. *Proc. Natl. Acad. Sci. U. S. A.* **2001**, *98*, 3404−3409. (e) Dinkova-Kostova, A. T.; Talalay, P. *Carcinogenesis* **1999**, *20*, 911−914.
(16) Los, G. V.; Encell, L. P.; McDougall, M. G.; Hartzell, D. D.; Karassina, N.; Zimprich, C.; Wood, M. G.; Learish, R.; Ohana, R. F.; Urh, M.; Simpson, D.; Mendez, J.; Zimmerman, K.; Otto, P.; Vidugiris, G.; Zhu, J.; Darzins, A.; Klaubert, D. H.; Bulleit, R. F.; Wood, K. V. *ACS Chem. Biol.* **2008**, *3*, 373−382.
(17) Rostovtsev, V. V.; Green, L. G.; Fokin, V. V.; Sharpless, K. B. *Angew. Chem., Int. Ed.* **2002**, *41*, 2596−2599.
(18) Williamson, A. *Philos. Mag.* **1850**, *37*, 350−356.
(19) (a) Jones, P. B.; Brinson, R. G.; Sarma, S. J.; Elkazaz, S. *Org. Biol. Chem.* **2008**, *6*, 4204−4211. (b) Blankespoor, R. L.; Smart, R. P.; Batts, E. D.; Kiste, A. A.; Lew, R. E.; Vander Vliet, M. E. *J. Org. Chem.* **1995**, *60*, 6852−6859.
(20) (a) Dinkova-Kostova, A. T.; Talalay, P.; Sharkey, J.; Zhang, Y.; Holtzclaw, W. D.; Wang, X. J.; David, E.; Schiavoni, K. H.; Finlayson, S.; Mierke, D. F.; Honda, T. *J. Biol. Chem.* **2010**, *285*, 33747−33755. (b) Cleasby, A.; Yon, J.; Day, P. J.; Richardson, C.; Tickle, I. J.; Williams, P. A.; Callahan, J. F.; Carr, R.; Concha, N.; Kerns, J. K.; Qi, H.; Sweitzer, T.; Ward, P.; Davies, T. G. *PLoS One* **2014**, *9*, e98896.
(21) Itoh, K.; Mochizuki, M.; Ishii, Y.; Ishii, T.; Shibata, T.; Kawamoto, Y.; Kelly, V.; Sekizawa, K.; Uchida, K.; Yamamoto, M. *Mol. Cell. Biol.* **2004**, *24*, 36−45. (b) Gayarre, J.; Stamatakis, K.; Renedo, M.; Perez-Sala, D. *FEBS Lett.* **2005**, *579*, 5803−5808. (c) Oh, J. Y.; Giles, N.; Landar, A.; Darley-Usmar, V. *Biochem. J.* **2008**, *411*, 297−306.
(22) Mitsunobu, O.; Yamada, Y. *Bull. Chem. Soc. Jpn.* **1967**, *40*, 2380−2382.
(23) In *Protein−Ligand Interactions*; Gohlke, H., Mannhold, R., Kubinyi, H., Folkers, G., Eds.; Wiley-VCH: Weinheim, 2012.
(24) (a) Barycki, J. J. In *Redox Biochemistry*; Banerjee, R., Ed.; Wiley Interscience: Hoboken, NJ, 2007; pp 11−21. (b) Ketterer, B.; Coles, B.; Meyer, D. J. *Environ. Health Perspect.* **1983**, *49*, 59−69. (c) Balogh, L. M.; Roberts, A. G.; Shireman, L. M.; Greene, R. J.; Atkins, W. M. *J. Biol. Chem.* **2008**, *283*, 16702−16710.
(25) (a) McGrath, C. E.; Tallman, K. A.; Porter, N. A.; Marnett, L. J. *Chem. Res. Toxicol.* **2011**, *24*, 357−370. (b) Kobayashi, M.; Li, L.; Iwamoto, N.; Nakajima-Takagi, Y.; Kaneko, H.; Nakayama, Y.; Eguchi, M.; Wada, Y.; Kumagai, Y.; Yamamoto, M. *Mol. Cell. Biol.* **2009**, *29*, 493−502. (c) Kansanen, E.; Bonacci, G.; Schopfer, F. J.; Kuosmanen, S. M.; Tong, K. I.; Leinonen, H.; Woodcock, S. R.; Yamamoto, M.; Carlberg, C.; Yla-Herttuala, S.; Freeman, B. A.; Levonen, A.-L. *J. Biol. Chem.* **2011**, *286*, 14019−14027. (d) pp 257−261 in ref 1a.
(26) (a) Wang, T.-Z.; Paquette, L. A. *J. Org. Chem.* **1986**, *51*, 5232−5234. (b) Gerber, P.; Keese, R. *Tetrahedron Lett.* **1992**, *33*, 3987−3988.
(27) (a) O'Neill, L. A. J. *Nat. Rev. Drug Discovery* **2006**, *5*, 549−563. (b) Dueber, J. E.; Yeh, B. J.; Bhattacharyya, R. P.; Lim, W. A. *Curr. Opin. Struct. Biol.* **2004**, *14*, 690−700. (c) Lim, W.; Mayer, B.; Pawson, T. In *Cell Signaling*; Garland Science: New York, 2014.
(28) Hynes, N. E.; Ingham, P. W.; Lim, W. A.; Marshall, C. J.; Massague, J.; Pawson, T. *Nat. Rev. Mol. Cell. Biol.* **2013**, *14*, 393−398.
(29) Reddy, A. S.; Zhang, S. *Expert Rev. Clin. Pharmacol.* **2013**, *6*, 41−47.

DOI: 10.1021/ja5132648
J. Am. Chem. Soc. 2015, 137, 6232−6244